

# Quantifying uncertainty in area and regression coefficient estimation from remote sensing maps

Kerri Lu<sup>\*1,2</sup>, Stephen Bates<sup>\*1,2</sup>, and Sherrie Wang<sup>\*1,3,4</sup>

<sup>1</sup>Laboratory for Information and Decision Systems, MIT

<sup>2</sup>Department of Electrical Engineering and Computer Science, MIT

<sup>3</sup>Department of Mechanical Engineering, MIT

<sup>4</sup>Institute for Data, Systems, and Society, MIT

## Abstract

Remote sensing map products are used to obtain estimates of environmental quantities, such as deforested area or the effect of conservation zones on deforestation. However, the quality of map products varies, and — because maps are outputs of complex machine learning algorithms that take in a variety of remotely sensed variables as inputs — errors are difficult to characterize. Without capturing the biases that may be present, naive calculations of population-level estimates from such maps are statistically invalid. In this paper, we compare several uncertainty quantification methods — stratification, Olofsson area estimation method, and prediction-powered inference — that combine a small amount of randomly sampled ground truth data with large-scale remote sensing map products to generate statistically valid estimates. Applying these methods across four remote sensing use cases in area and regression coefficient estimation, we find that they result in estimates that are more reliable than naively using the map product as if it were 100% accurate and have lower uncertainty than using only the ground truth and ignoring the map product. Prediction-powered inference uses ground truth data to correct for bias in the map product estimate and (unlike stratification) does not require us to choose a map product before sampling. This is the first work to (1) apply prediction-powered inference to remote sensing estimation tasks, and (2) perform uncertainty quantification on remote sensing regression coefficients without assumptions on the structure of map product errors. To improve the utility of machine learning-generated remote sensing maps for downstream applications, we recommend that map producers provide a holdout ground truth dataset to be used for calibration in uncertainty quantification alongside their maps. Data and code are available at <https://github.com/Earth-Intelligence-Lab/uncertainty-quantification>.

## 1 Introduction

Remote sensing maps are widely used to obtain estimates for environmental quantities [16, 4, 28, 38, 9]. Map products created by training machine learning models on remotely sensed data allow researchers to cheaply access predictions for a variable of interest at a high resolution over large regions.

However, the quality of map products varies, and resulting population-level estimates of quantities of interest may be biased and statistically invalid [19, 5, 36]. For example, [5] showed that human labeling of high-resolution imagery results in an estimate of global forest extent in dryland biomes that is 40% to 47% higher than previous estimates from remotely sensed forest cover map products. Moreover, different map products may conflict with each other and result in significantly different estimates over the same region. For example, [1] found that two commonly used satellite-based remote sensing maps of forest cover in Mexico differ significantly from each other, implying that there is misclassification error in at least one of the algorithms used to categorize pixels as forest or non-forest. Another recent study of three satellite-based global land cover/land use map products found that the maps are biased toward different land cover classes

---

\*Email: {kerrilu, stephenbates, sherriwang}@mit.edu

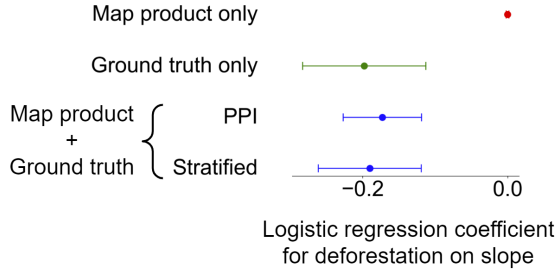


Figure 1: **Motivating example: map-only inference is statistically invalid.** The 95% confidence interval for logistic regression coefficient relating Brazilian Amazon deforestation to slope using  $N = 963548$  remote sensing map points and  $n = 1386$  ground truth points. The imputed slope coefficient from the map alone falls outside the confidence intervals for all methods that use ground truth points.

(e.g., one map overestimates shrub cover and another overestimates grass cover relative to the other maps) [37].

Additionally, errors in map products are often difficult to characterize due to the complexity of input data and lack of interpretability in the ML models used to generate the maps. Examples of systematic errors in map products trained on satellite data include “nonrandom misclassification, saturation effects, atmospheric effects, and cloud cover,” all of which may lead to biased inference [19]. This has prevented environmental scientists, economists, and policymakers from using remote sensing maps in their analyses. The World Bank has cited uncertainty in remote sensing maps as a barrier to their use in water resources management [15], and the United Nations Task Team on Satellite Imagery and Geospatial Data wrote that the “shift in paradigm from traditional statistical methods (e.g., counting, measuring by humans) towards estimation from sensors (with associated aspects of validity, approximation, uncertainty)... will require convincing, statistically sound results” [18]. Correctly accounting for map errors, then, is crucial for maximizing the potential of remote sensing data to expand scientific knowledge and advance practical operations.

For those who currently reject estimation from remote sensing as too unreliable, the alternative is to use ground truth observations for the variable of interest. However, ground truth data is often sparse because it is expensive to collect, as it may require fieldwork or manual labelling of remote sensing imagery. Few ground truth points result in greater uncertainty (e.g., wider confidence intervals) in estimates. Another alternative is to use both ground truth data and remote sensing maps to generate estimates, using the ground truth points to correct for biases that may exist in the map products. This generally reduces uncertainty in the estimates compared to using ground truth alone, since map products contain a large amount of data that, while possibly biased, still give useful information about the true values we wish to measure.

**A motivating example.** In this work, we discuss methods that correct map products with ground-truth data to give statistically-valid confidence intervals. We give a brief preview here. We seek to estimate logistic regression coefficients for the association between Brazilian Amazon deforestation in 2000–2015 and several covariates, including terrain slope. Using nearly one million remote sensing map product points and 1386 ground truth points, we compare the 95% confidence intervals for the slope coefficient with four methods (Figure 1) described shortly. See Section 4.1 for a complete description of the experimental setup.

The “classical” estimate using only ground truth points is statistically valid but has the widest confidence interval, failing to take advantage of existing map products. Meanwhile, methods that use a map product along with the ground truth points produce an estimate with lower uncertainty while still being valid.

Notably, the slope coefficient computed from the map product alone (“naive imputation”) is approximately zero, which falls outside the confidence intervals for all methods that use ground truth points. That is, if we had used only the map product, we would not have discovered the statistically significant negative relationship between slope and deforestation. Methods like PPI allow us to use ground truth points to correct for bias in the map product and thus avoid misleading conclusions.

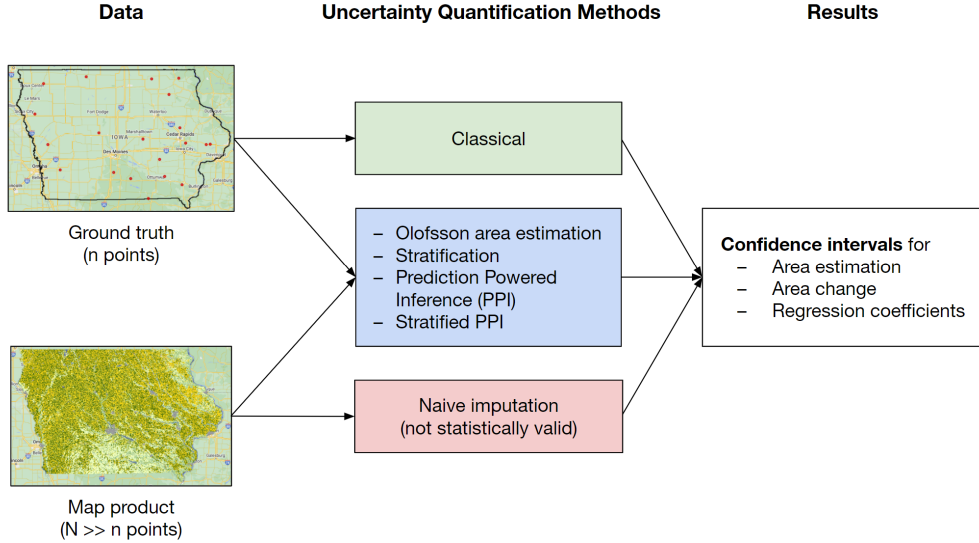


Figure 2: **Overview of uncertainty quantification using ground truth data and remote sensing map products.** Olofsson area estimation, stratification, and prediction powered inference methods use a small amount of ground truth data along with a map product to produce confidence intervals for the quantity of interest. We also compare these methods against classical uncertainty quantification (using only ground truth) and naive imputation (using only the map product).

**Our contribution.** In this paper, we consider uncertainty quantification methods that combine a small number of randomly sampled ground truth data ( $n$  points) with large-scale remote sensing map products ( $N$  points, where  $N$  is much larger than  $n$ ) in order to generate statistically valid estimates with low uncertainty (Figure 2). **Stratification** uses map products to determine a sampling strategy for ground truth points that reduces the variance of estimates; it has been used in the remote sensing community for decades [17, 11, 32, 26]. **Prediction-powered inference (PPI)** [3, 2] is a recently developed uncertainty quantification method that uses a small set of ground truth points to calibrate and correct for bias in a much larger set of ML-generated predictions, resulting in more precise estimates than using the ground truth points alone. We compare stratification and prediction-powered inference against classical estimation (using only ground truth) and naive imputation (using only a map product).

We apply these methods to two of the most common scientific uses of remote sensing maps: **area estimation** and **regression coefficient estimation**. Area estimation includes estimating both total area occupied by a land cover/land use category and total change in land cover/land use over time. The methods applied to area estimation also apply to estimating sums or averages of continuous variables, such as total carbon stock. Regression coefficient estimation refers to estimating linear or logistic regression coefficients for causal or associative relationships between two or more environmental variables. For regressions, this paper only accounts for uncertainty in the remotely sensed dependent variable, while the covariates are assumed to have no errors. To illustrate the methods, we consider four specific remote sensing estimation tasks spanning crop area estimation, deforestation quantification, and associating deforestation and tree cover to other geophysical variables; see Table 1. Data and code for these use cases are available at <https://github.com/Earth-Intelligence-Lab/uncertainty-quantification>.

Combining ground truth data with map products results in statistically valid estimates that are more reliable than naive imputation and have lower uncertainty than classical estimates. As we will show, naive imputation from maps without bias correction can result in completely incorrect area and regression coefficient estimates. To improve the utility of machine learning-generated remote sensing maps for downstream applications, we recommend that map *producers* provide a holdout ground truth dataset (such as the usual test set) to be used for calibration in uncertainty quantification alongside their maps, or, if that is not done, for map *users* to generate their own holdout set for calibration, if possible (e.g., from visual inspection of remote sensing data).

Estimation task	Target variable	Region	Year	Map product(s)	Ground truth	Covariates	Link to code
Area	Maize	Iowa	2022	USDA NASS Cropland Data Layers (CDL) [25]	Simulated	N/A	<a href="#">link</a>
Area	Deforestation	Brazilian Amazon	2000-2015	1. NASA Global Forest Cover Change [33] 2. Amazon ecoregion deforestation strata [7]	$n = 1386$ from [7]	N/A	<a href="#">link</a>
Logistic regression coefficients						Distance from roads, distance from rivers, elevation, slope	<a href="#">link</a>
Linear regression coefficients	Tree cover	Contiguous USA	2021	USFS Tree Cover [12]	$n = 983$ manually labelled Google Maps high-resolution satellite images	Aridity index, elevation, slope	<a href="#">link</a>

Table 1: **Overview of use cases and datasets.** We estimate maize area in Iowa, deforestation area and logistic regression coefficients in the Brazilian Amazon, and tree cover linear regression coefficients in the United States. The Iowa maize area use case is a simulation: we treat a small random sample of CDL map product points as “ground truth” data and observe the effects of artificially degrading the map product relative to the ground truth. Code implementations of the use cases are linked in the rightmost column.

**Related work.** Previously, Olofsson *et al.* [27] described an area estimation method that uses the confusion matrix between land cover ground truth and map product points to correct for misclassification bias in the map product. The Olofsson method is commonly used in the remote sensing community to generate confidence intervals for area estimates. However, it does not apply to regression coefficient estimation tasks. One contribution of the present work is a comparison of this method and PPI. We find both experimentally and mathematically that these two methods produce similar outputs for area estimation.

Other methods have been developed to reduce bias in regression coefficient estimates from remote sensing data. For example, [1] estimates the effect of a conservation program on deforestation in Mexico. They correct for bias in the remotely sensed deforestation binary variable by modelling misclassification error as dependent on environmental covariates via a logit model. Another study [13] estimates logistic regression coefficients for the relationship between roads and forest cover in West Africa. They train an adversarial debiasing model with ground truth data to correct for bias arising from correlations between distance from roads and the measurement error in remotely sensed forest cover. Another study [29] uses co-located ground truth and remotely sensed data to show that using remote sensing data alone leads to biased regression coefficient estimates for several effect size estimation tasks in the US. They use a linear measurement error model and apply multiple imputation: a statistical method that uses a small amount of ground truth data to estimate remote sensing measurement error and impute corrected values for remotely-sensed variables. Note that this method requires an assumption about the error structure of the remotely-sensed variables, whereas the methods investigated herein do not.

Another approach to uncertainty quantification is *conformal prediction*, which generates statistically valid confidence sets for machine learning predictions at individual data points. For example, [35] applies conformal prediction to quantify pixel-level uncertainty for a land cover/land use map product in the Brazilian Amazon, outputting a 90% predictive set of land cover classes for each pixel (i.e., the set contains the true land cover class 90% of the time). This approach differs from our work because our methods estimate total area and regression coefficients over an entire region, rather than quantifying uncertainty at individual points or pixels.

Unlike previous works, this paper is the first work to apply prediction-powered inference to remote sensing use cases in area and regression coefficient estimation. Unlike stratified random sampling, PPI does not require that ground truth points be sampled according to a pre-determined stratification map; as a result, it allows for greater flexibility in ground truth data usage across different downstream applications. Additionally, this is the first work to combine map product and ground truth data to perform uncertainty quantification on remote sensing regression coefficients without assuming an error structure on the map product predictions.

Method	Data Used		Statistically Valid?	Caveats
	Map	Ground Truth		
Naive imputation	✓	✗	✗	
Classical	✗	✓	✓	
Stratification	✓	✓	✓	Ground truth points sampled using stratified map
Olofsson	✓	✓	✓	Area estimation only
PPI	✓	✓	✓	

Table 2: **Summary of uncertainty quantification methods.** PPI is the most flexible method that incorporates both ground truth and map product data.

## 2 Background: Uncertainty Quantification

We formally describe uncertainty quantification methods that generate confidence intervals with remote sensing variables. As two baselines, we first consider methods that use only the ground-truth data (which is valid but loses information) or only use the remote-sensing data (which is not statistically valid). We then turn to methods that use both sources of data to produce statistically-valid confidence intervals. See Table 2 for a summary.

### 2.1 Baseline methods

**Classical: use only the ground-truth data.** First, **classical** uncertainty quantification uses ground truth observations, sampled uniformly at random, to estimate the quantity of interest. For example, suppose there is a target variable  $Y$  that can be observed over a given area, and we wish to generate a 95% confidence interval for its population mean  $\theta^* = E[Y]$ . If we have  $n$  ground truth observations  $Y_1, Y_2, \dots, Y_n$  sampled uniformly at random, we can compute the sample mean

$$\hat{\theta} = \frac{1}{n} \sum_{i=1}^n Y_i$$

and standard error

$$SE = \sqrt{\frac{1}{n} \text{Var}(Y_i)} = \frac{1}{n} \sqrt{\sum_{i=1}^n (Y_i - \hat{\theta})^2}$$

to produce the classical 95% confidence interval

$$C = (\hat{\theta} - 1.96 \cdot SE, \hat{\theta} + 1.96 \cdot SE).$$

This method is conservative — if the size  $n$  of the ground truth dataset is small, the classical confidence interval will be large.

**Naive imputation: use only the remote sensing map.** If we have a remote sensing data product with a large number  $N$  of predictions  $\hat{Y}_1, \hat{Y}_2, \dots, \hat{Y}_N$  over the area of interest, we could treat these predictions like ground truth points and use the formula above with  $\hat{Y}$  in place of  $Y$ . This would produce a much smaller confidence interval, since we would use  $N$  instead of  $n$  in the denominator of the standard error. However, this **naive imputation** approach is not statistically valid, as it does not account for error or uncertainty in the model used to generate the map product predictions.

## 2.2 Stratification

**Stratified random sampling** uses remotely sensed maps to determine a sampling strategy for ground truth points that reduces the variance of estimates. Stratification is commonly used in the remote sensing community.

We first use a map product to partition the area of interest into  $K$  strata (sub-areas) such that the target variable is predicted to have low variance within each stratum. Then we sample  $n_k$  ground truth points uniformly at random from each stratum  $1 \leq k \leq K$ . We can choose  $n_k$  to be larger for strata predicted to have higher uncertainty to decrease the standard error within the strata and hence make the overall standard error smaller with the same total number of samples.

Suppose we again wish to estimate  $\theta^* = E[Y]$  using a stratified random sample. For each stratum  $k$ , we compute the stratum sample mean  $\hat{\theta}_k$  and stratum standard error  $SE_k$  using the same formulae as the classical method. Suppose that in the map product, each stratum  $k$  takes up proportion  $0 < A_k < 1$  of the total area. Then, we compute the stratified mean

$$\hat{\theta}_{\text{strat}} = \sum_{k=1}^K A_k \hat{\theta}_k$$

and stratified standard error

$$SE_{\text{strat}} = \sqrt{\sum_{k=1}^K A_k^2 \cdot SE_k^2}$$

to produce the stratified 95% confidence interval

$$C_{\text{strat}} = (\hat{\theta}_{\text{strat}} - 1.96 \cdot SE_{\text{strat}}, \hat{\theta}_{\text{strat}} + 1.96 \cdot SE_{\text{strat}}).$$

The advantage of stratification with an accurate map and well-chosen sampling strategy is that the variance within each stratum will be small, which results in a smaller overall confidence interval compared to the classical method. If the map predictions are inaccurate, then the ground truth points likely have higher variance within each map stratum, resulting in a larger confidence interval. Thus the uncertainty quantification incorporates the accuracy of the map product predictions.

For example, in our Brazilian Amazon deforestation area estimation use case, we use a remotely sensed stratification map created by [7] using Landsat surface reflectance imagery at 30 m resolution. The map (Figure 3) partitions the Amazon into seven strata related to forest change from 1995-2017: stable forest, stable non-forest, deforestation, natural disturbance, natural disturbance and deforestation, regrowth, and buffer. The strata are designed so that points within each stratum have low variance in deforestation status (for instance, most points in the “stable forest” and “stable non-forest” strata do not experience deforestation in the time period of interest). As a result, our stratified confidence interval for deforestation area is smaller than the classical confidence interval.

## 2.3 Prediction-Powered Inference

Prediction-powered inference (PPI) [3] is an uncertainty quantification method that computes confidence intervals using a small set of ground truth points and a much larger set of machine learning generated predictions. While stratified sampling requires us to commit to a map product and stratification scheme before sampling the ground truth points, the map product used in PPI can be chosen after sampling. The main idea is that PPI assesses the bias in the map product using the ground truth data and then corrects it.

PPI evaluates the accuracy of the map product by comparing the ground truth labels  $Y_1, Y_2, \dots, Y_n$  to the map product predictions  $\hat{Y}_1, \hat{Y}_2, \dots, \hat{Y}_n$  at the corresponding ground truth point locations. For a concrete example, suppose we wish to estimate  $\theta^* = E[Y]$  as before. The PPI point estimate is

$$\hat{\theta}_{\text{PPI}} = \underbrace{\frac{1}{N} \sum_{i=1}^N \hat{Y}'_i}_{\text{naive imputation}} - \underbrace{\frac{1}{n} \sum_{i=1}^n (\hat{Y}_i - Y_i)}_{\text{bias correction}}.$$

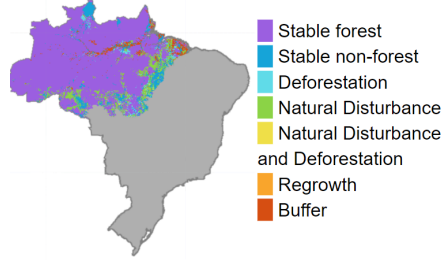


Figure 3: **Stratified random sample is a standard approach for estimation with remote sensing maps.** This example shows a map of the Brazilian Amazon used for stratification. The strata are designed so that points within each stratum have low variance in deforestation status, which reduces the uncertainty when estimating area deforested. Adapted from [7].

The PPI standard error is

$$\begin{aligned} SE_{\text{PPI}} &= \sqrt{\frac{1}{N} \text{Var}(\hat{Y}'_i) + \frac{1}{n} \text{Var}(\hat{Y}_i - Y_i)} \\ &\approx \sqrt{\frac{1}{n} \text{Var}(\hat{Y}_i - Y_i)}, \end{aligned}$$

where the approximation holds when  $N$  is much larger than  $n$ . This yields the PPI 95% confidence interval,

$$C_{\text{PPI}} = (\hat{\theta}_{\text{PPI}} - 1.96 \cdot SE_{\text{PPI}}, \hat{\theta}_{\text{PPI}} + 1.96 \cdot SE_{\text{PPI}}).$$

The first term in  $SE_{\text{PPI}}$  is the variance corresponding to using only map predictions to estimate  $\theta$ , i.e.  $\frac{1}{N} \text{Var}(\hat{Y}'_i)$ . The second term is the variance from the bias correction,  $\frac{1}{n} \text{Var}(\hat{Y}_i - Y_i)$ . As the number of map product points  $N$  grows large,  $SE_{\text{PPI}}$  approaches  $\sqrt{\frac{1}{n} \text{Var}(\hat{Y}_i - Y_i)}$ . This will be a realistic approximation in many cases, since remote sensing maps at a global, national, or province level can contain millions or even billions of pixels, whereas the number of ground truth points  $n$  is commonly in the hundreds or thousands. The greater the accuracy of the map product, the smaller  $\text{Var}(\hat{Y}_i - Y_i)$  will be and the smaller the PPI confidence interval will be. Note that the PPI confidence interval is smaller than the classical confidence interval if  $\text{Var}(\hat{Y}_i - Y_i) < \text{Var}(Y_i)$ , which will be true for any map whose predictions correlate positively with the ground truth.

PPI can also give confidence intervals for linear and logistic regression coefficients, but the formulae are more complex. We sketch the main idea here and refer the reader to [2, 3] for a full exposition. In brief, PPI begins like naive imputation by using a large set of map predictions  $\hat{Y}'_1, \hat{Y}'_2, \dots, \hat{Y}'_N$  to compute a **measure of fit**  $m_\theta$ . Then, PPI computes a **bias correction**  $\Delta_\theta$  by comparing the ground truth data  $Y_i$  to the predictions  $\hat{Y}_i$ . The relevant formula for the measure of fit and bias correction depends on what we seek to estimate — areas, binary regression coefficients, linear regression coefficients, etc. — see Table 3. Lastly, the naive  $m_\theta$  and the bias correction  $\Delta_\theta$  are combined to construct the PPI 95% confidence interval

$$C_{\text{PPI}} = \{\theta : |m_\theta + \Delta_\theta| \leq w_\theta\}$$

where  $w_\theta$  is a constant that depends on the confidence level (95% in this case).

PPI can be used with either uniform random sampling or stratified random sampling of the ground truth points [10]. **Stratified (weighted) PPI** can be applied as follows for mean estimation. Each ground truth value  $Y_i$  and labeled prediction  $\hat{Y}_i$  is multiplied by weight  $w_i = A_k \frac{n}{n_k}$  where  $k$  is the stratum where point  $i$  is located,  $A_k$  is the area proportion of stratum  $k$  and  $n_k$  is the number of ground truth samples in stratum  $k$ . Similarly, each unlabeled prediction  $\hat{Y}'_i$  in stratum  $k$  is multiplied by weight  $w_i = A_k \frac{N}{N_k}$  where  $N_k$  is the number of map product points in stratum  $k$ . Then the same PPI formulae as above can be used.

We use the PPI-PYTHON software package to implement the unweighted and weighted versions of PPI for our use cases. The software includes a tuning parameter  $\lambda$  that we set using the map product points and ground-truth points. The confidence intervals are statistically valid even with this data-driven tuning [2].

Estimand	Measure of fit $m_\theta$	Bias correction $\Delta_\theta$
Mean	$\theta - \frac{1}{N} \sum_{i=1}^N \hat{Y}'_i$	$\frac{1}{n} \sum_{i=1}^n (\hat{Y}_i - Y_i)$
Logistic regression	$\frac{1}{N} \sum_{i=1}^N \left( \frac{X'_i}{1+e^{-\theta^T X'_i}} - \hat{Y}'_i \right)$	$\frac{1}{n} \sum_{i=1}^n X_i (\hat{Y}_i - Y_i)$
Linear regression	$\theta - (X')^\dagger \hat{Y}'$	$X^\dagger (\hat{Y} - Y)$

Table 3: **Prediction-powered inference (PPI) formulae** for three common estimation tasks found in remote sensing: mean estimation, logistic regression coefficients, and linear regression coefficients.

## 2.4 Olofsson *et al.* (2013) area estimation

Olofsson *et al.* [27] introduces an uncertainty quantification method that uses the confusion matrix between ground truth and map product land cover labels to estimate the area of a land cover class. This method is commonly used in the remote sensing community. Like PPI, the Olofsson method computes confidence intervals by using ground truth points to correct for bias in the map product estimates. In fact, we show mathematically in Appendix A that the two methods result in similar confidence intervals as the number of map product points  $N$  grows large. However, unlike PPI, the Olofsson method only applies to area estimation but not regression coefficient estimation.

Turning to the method, suppose we have a map product with  $K$  land cover classes, as well as  $n$  randomly sampled ground truth points. The Olofsson method constructs the  $K \times K$  misclassification confusion matrix between ground truth points and map product predictions at the ground truth point locations. For each  $1 \leq i \leq K$  and  $1 \leq j \leq K$ , let  $n_{ij}$  denote the number of points that are in map class  $i$  and ground truth class  $j$ . For each class  $1 \leq i \leq K$ , let  $0 < A_i < 1$  denote the proportion of the total map area taken up by the map class.

Then, the area estimate for the area of class  $j$  is

$$\hat{\theta}_{j, \text{Olofsson}} = \sum_{i=1}^K A_i \frac{n_{ij}}{n_i}$$

with corresponding standard error

$$SE_{j, \text{Olofsson}} = \sqrt{\sum_{i=1}^K A_i^2 \frac{\frac{n_{ij}}{n_i} (1 - \frac{n_{ij}}{n_i})}{n_i}}.$$

The 95% confidence interval for the area of class  $j$  is

$$C_{j, \text{Olofsson}} = (\hat{\theta}_{j, \text{Olofsson}} - 1.96 \cdot SE_{j, \text{Olofsson}}, \hat{\theta}_{j, \text{Olofsson}} + 1.96 \cdot SE_{j, \text{Olofsson}}).$$

Area estimation is a special case of mean estimation in which we estimate the mean of a binary variable that is 1 for all points in class  $j$  and 0 for all points outside of class  $j$ . Thus, we can also perform area estimation using methods such as PPI and stratification. If the  $n$  ground truth points are obtained by stratified random sampling using the  $K$  map land cover classes as the strata, the Olofsson confidence interval is identical to the stratified confidence interval.

## 2.5 Evaluating performance using effective sample size

We use **effective sample size** to compare the effectiveness of uncertainty quantification methods. Suppose a classical confidence interval of width  $w$  is generated using  $n$  ground truth points. If another uncertainty quantification method uses  $n$  ground truth points (along with a map product) to generate a confidence interval of width  $w'$ , then the effective sample size of the new method is

$$n_{\text{effective}} = n \cdot \left( \frac{w}{w'} \right)^2.$$

This is the number of ground truth points that would be required to generate a classical confidence interval of width  $w'$ .

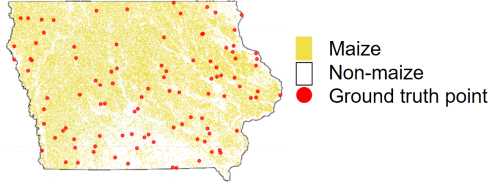


Figure 4: **Iowa maize area estimation datasets.** The Iowa maize binary map product is derived from the USDA’s Cropland Data Layer, and  $n = 100$  uniformly randomly sampled “ground truth points” are shown.

### 3 Area estimation

In this section, we demonstrate uncertainty quantification for two area estimation use cases. First, we simulate estimating maize area in Iowa in 2022, artificially degrading the map product quality relative to simulated “ground truth” points, in order to observe the effect of map product noise and bias on the area estimate under different methods. We will see through this simulation the importance of bias correction before using maps to estimate total area. We then use real ground truth data and real map products developed by researchers to estimate change in tree cover in the Brazilian Amazon in 2000–2015. We compare the classical method, naive imputation, stratification, PPI, stratified PPI, and the method of Olofsson *et al.* (2013) [27].

In each use case, we use binary data where each point has value 1 if it belongs to the land cover class of interest (e.g., cropland or deforested land), and value 0 otherwise. Then, estimating the area fraction of the land cover class is equivalent to estimating the mean of all points in the region.

#### 3.1 Simulation: Maize area in Iowa

**Problem Formulation** We simulate estimating the fraction of maize area in Iowa in 2022. To probe the effect of map product noise and bias on different methods, we artificially degrade the map product quality relative to simulated “ground truth” points, as described next.

For this simulation, we use the USDA’s Cropland Data Layer (CDL) [25] as the ground truth for crop types in Iowa. CDL is a crop type land cover map created using satellite imagery and agricultural ground truth data in the continental United States. It has 94.2% producer’s accuracy and 97.2% user’s accuracy for the maize land cover class in Iowa. We sample  $N = 100000$  locations uniformly at random from a binary maize/non-maize map derived from CDL (Figure 4). The mean of the 100000 map product points is 0.35, which we will consider the “true” fraction of maize for the simulation.

In each trial, we sample  $n = 100$  “ground truth” points uniformly at random from the  $N = 100000$  map product points. Initially, we set the map product and ground truth equal to each other at the 100 ground truth locations. We then experiment with degrading the map product quality as follows. We systematically add noise or bias to the map product points while keeping the ground truth points constant, and then compare our maize fraction estimates across naive imputation, classical estimation, and PPI. We average results over 100 trials.

**Adding unbiased noise.** We define adding unbiased noise at level  $p$  to the map product as resampling each of the 100000 map product points with probability  $p$  from the Bernoulli(0.35) distribution. In other words, about  $p$  fraction of the points are randomly labeled, while the remaining  $1 - p$  points are unchanged. Each resampled point is labeled as maize with probability 0.35 and non-maize with probability 0.65. We experiment with noise probabilities  $p$  from 0 to 1 at increments of 0.1.

**Adding bias.** We also consider adding bias to the map product. Here, we define adding bias  $p$  to the map product as resampling each of the 100000 map product points with probability 0.4 from the Bernoulli( $p$ ) distribution. In other words, about 40% of the points are randomly labeled, while the remaining 60% points are unchanged. Each resampled point is labeled as maize with probability  $p$  and non-maize with probability  $1 - p$ . We experiment with bias values  $p$  from 0 to 1 at increments of 0.1. When  $p = 0.35$ , this does not add bias, but as  $p$  ranges farther from 0.35, the amount of bias increases.

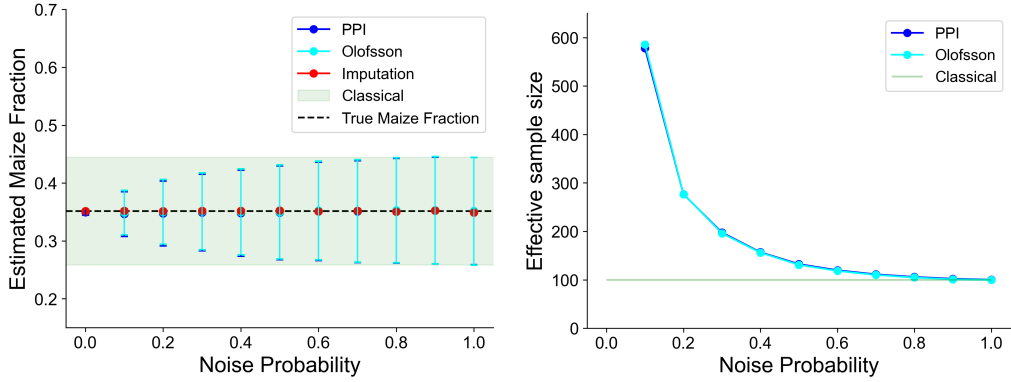


Figure 5: **Simulation estimating maize fraction under different levels of map noise** using  $N = 100000$  map product points and  $n = 100$  “ground truth” points. Olofsson and PPI results are overlapping. Left: Maize fraction 95% confidence intervals at different noise levels. Right: Maize fraction effective sample size at different noise levels. (At noise level  $p$ , about  $p$  fraction of the points are resampled, while the remaining  $1 - p$  points are unchanged. Each resampled point is labeled as maize with probability 0.35 (the true maize fraction) and non-maize with probability 0.65.)

**Results** As we add increasing amounts of random noise to the map, all confidence intervals for maize area remain centered at the true maize fraction of 0.35 (Figure 5). This is what we expect, since our noise-adding process resamples from the Bernoulli(0.35) distribution, causing the overall fraction of maize to remain the same. The classical confidence interval stays constant because it only uses ground truth points. The map-based imputation confidence intervals are small because  $N = 100000$  is large, but they do not account for error in the map product. However, the imputation confidence intervals remain unbiased because the map still has true maize fraction close to 0.35 regardless of noise level.

When the noise probability is low, the PPI confidence intervals are significantly smaller than the classical intervals. This is because the error of the map product ( $\hat{Y} - Y$ ) is small at the ground truth locations, so the variance of this error is also small, resulting in a small PPI standard error. As noise increases, the variance of the error of the map product increases; the PPI confidence intervals grow wider, eventually converging to the classical confidence interval at noise probability  $p = 1$ . (At  $p = 1$ , the map is complete noise and therefore does not provide any information for estimating the area beyond the information contained in the ground truth samples.) Consequently, the PPI effective sample size decreases from  $n_{\text{effective}} = 578$  when  $p = 0.1$  to  $n_{\text{effective}} = 100$  when  $p = 1$  (which matches the number of actual ground truth points  $n = 100$ ). Thus, the effectiveness of PPI is dependent on the quality of the map product. The Olofsson confidence intervals and effective sample sizes are nearly identical to those of PPI.

The estimated maize fraction confidence intervals after adding bias to the map product are shown in Figure 6. Again, the classical confidence interval stays constant and remains centered at the true maize fraction because it only uses the ground truth points. As bias increases, the fraction of map product points labeled as “maize” increases. As a result, the map-based imputation estimates increase with the bias value, and generally do not remain centered at the true maize fraction of 0.35. The imputation confidence intervals are small because  $N = 100000$  is large, but they are unreliable because they do not correct for the bias in the map product. In contrast, the PPI estimates remain centered at the true maize fraction because PPI corrects for bias in the map product. The PPI confidence intervals are smaller than the classical intervals because the variance of the map product error  $\hat{Y} - Y$  is small (since only about 40% of the map product points are resampled, regardless of bias level). Thus, PPI provides unbiased estimates with lower uncertainty than using only the ground truth points. Again, the Olofsson confidence intervals and effective sample sizes are nearly identical to those of PPI, as expected.

We also plot the maize fraction confidence intervals against model accuracy for both the noise and bias experiments (Figure 7). As noise increases, model accuracy decreases, so low model accuracy is associated with wide PPI and Olofsson confidence intervals. Thus, the left panel of Figure 7 resembles an inverted version of the left panel of Figure 5.

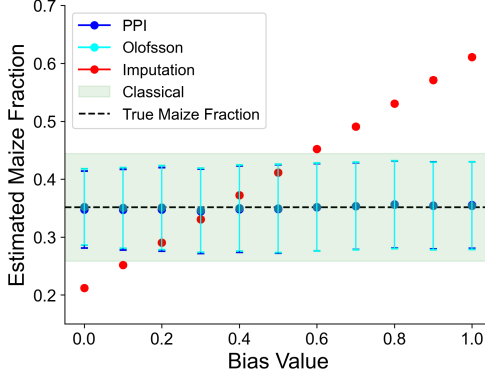


Figure 6: **Simulation estimating maize fraction 95% confidence intervals under different levels of map bias** using  $N = 100000$  map product points and  $n = 100$  “ground truth” points. Olofsson and PPI confidence intervals are overlapping. (Noise is fixed at 0.4 so about 40% of the points are resampled. At bias  $p$ , each resampled point is labeled as maize with probability  $p$  and non-maize with probability  $1 - p$ .)

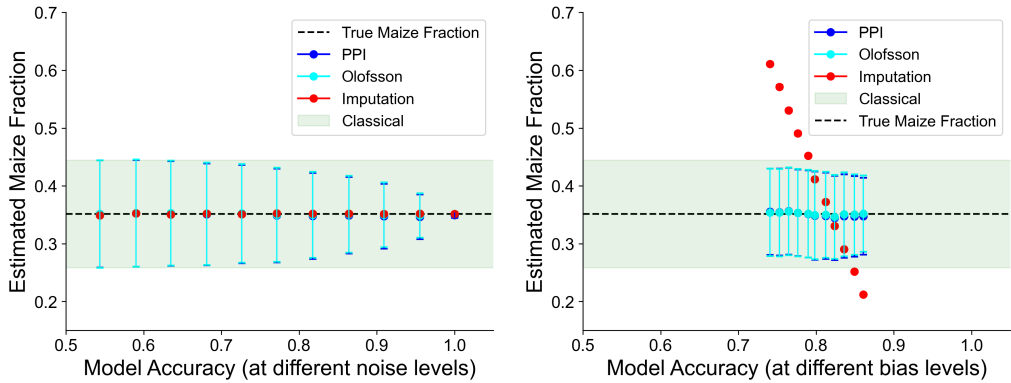


Figure 7: **Simulation estimating maize fraction 95% confidence intervals at different map product accuracy levels** obtained by varying noise (left) and bias (right), using  $N = 100000$  map product points and  $n = 100$  “ground truth” points. Olofsson and PPI confidence intervals are overlapping.

As bias increases and the fraction of map product points labeled as “maize” increases, model accuracy decreases linearly. (To see this, note that if each resampled point is labeled as maize with probability  $p$ , then an expected  $0.35(p) + 0.65(1 - p) = 0.65 - 0.3p$  fraction of the resampled points will match the ground truth.) Thus, the map-based imputation estimates of maize fraction decrease linearly as model accuracy increases. In the right panel of Figure 7, a model accuracy of 0.86 corresponds to an imputed maize fraction of 0.21, significantly lower than the true fraction of 0.35. This shows that even a map with high model accuracy can yield biased estimates under naive imputation.

### 3.2 Deforestation area in Brazilian Amazon

**Problem Formulation** Next, we move on to real data and estimate the fraction of deforestation in the Brazilian Amazon from 2000 to 2015, comparing confidence interval widths across methods.

We create a binary deforestation map product using all  $N = 4.4 \times 10^9$  pixels from the NASA Global Forest Cover Change (GFCC) map [33] (at 30 m resolution) in the study area (Figure 8). The GFCC product is derived from Landsat 5 and Landsat 7 surface reflectance imagery, and includes maps for tree cover percentage in each pixel in five-year increments from 2000 to 2015. We consider a map pixel deforested if its canopy cover percentage satisfies  $\text{canopy}_{2015} - \text{canopy}_{2000} \leq -25\%$  (Appendix B).

We use a ground truth Amazon deforestation and forest disturbance dataset created by [7] using time-

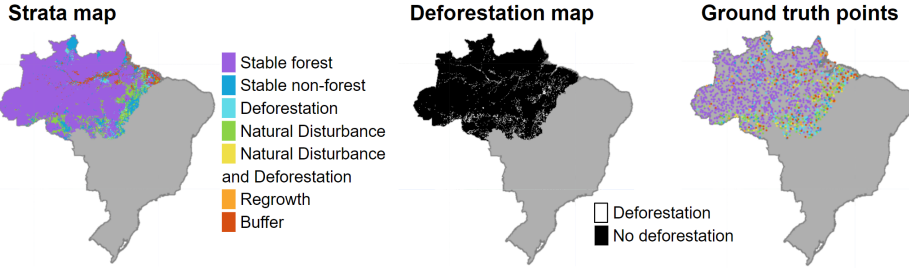


Figure 8: **Brazilian Amazon deforestation area estimation datasets.** Left: Stratification map from [7]. Center: Binary map of deforestation from 2000-2015 derived from NASA Global Forest Cover Change. Right:  $n = 1386$  ground truth points from [7], colored according to the stratum from which they are sampled.

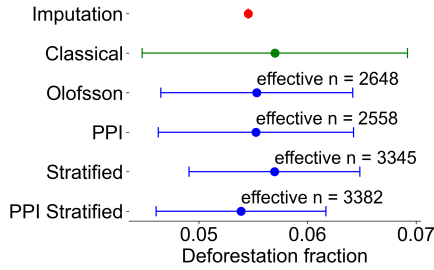


Figure 9: **Brazilian Amazon deforestation 95% confidence intervals** using  $N = 4.4 \times 10^9$  map product points and  $n = 1386$  ground truth points. The Olofsson confusion matrix method, PPI, and stratification all result in smaller confidence intervals for estimated deforestation than classical estimation, with Stratified PPI having the best performance.

series analysis of Landsat imagery and high-resolution imagery from Google Earth between 1995 and 2017. The dataset records the years corresponding to deforestation, degradation, and natural disturbance events at each ground truth point. We use this to construct a binary ground truth dataset restricted to Brazil, in which we consider a point deforested if it experienced a deforestation event between 2000 and 2015. The original dataset is obtained by stratified random sampling, using a stratification map (also created by [7]) that contains 7 strata related to deforestation status. To generate a classical estimate baseline, we construct a “uniformly random sampled” ground truth dataset by downsampling the points in each of the strata to match its area proportion. For a fair comparison, we also downsample the original stratified ground truth dataset to match the size of the “uniformly random” dataset. This results in two ground truth datasets of  $n = 1386$  points each, corresponding to uniform random sampling and stratified random sampling. Both ground truth datasets are used with PPI to obtain confidence intervals.

**Results** Each method results in a point estimate that between 5% to 6% of the Brazilian Amazon was deforested between 2000 and 2015. The Olofsson confusion matrix method, PPI, and stratification all result in smaller 95% confidence intervals for estimated deforestation than classical estimation (Figure 9). The Olofsson and PPI confidence intervals are fairly similar, with respective effective sample sizes that are 1.9 and 1.8 times the actual number of ground truth samples. The stratified and stratified PPI confidence intervals have the best performance, with effective sample sizes that outperform the classical method by a factor of about 2.4. (Put differently, stratified PPI has effective sample size 3382, so using the remotely sensed deforestation map added the equivalent of  $3382 - 1386 = 1996$  ground truth samples.) Thus, the methods that use both map product and ground truth reduce uncertainty in our estimates, compared to using only ground truth. In particular, stratification is effective because the strata map is designed so that points within each stratum have low variance in deforestation status.

In this case, the naive imputation estimate — using only the map to estimate deforestation without any bias correction via ground truth labels — falls within the other confidence intervals, suggesting that

the NASA Global Forest Cover Change map has small bias for estimating deforestation area. However, we emphasize that this would not have been clear without the ground truth data, and ground truth data is still necessary to check the reliability of the map product for deforestation analysis.

## 4 Estimating regression coefficients

In this section, we apply our uncertainty quantification methods to estimating regression coefficients for associative relationships between a remotely sensed outcome and multiple covariates. Regressions are commonly used in the environmental sciences and economics to identify relationships — associative or causal — between covariates and a binary outcome (logistic regression) or between covariates and a continuous outcome (linear regression). Logistic regression coefficients give the change in the log odds ratio of a binary outcome corresponding to a one-unit increase in a covariate. Linear regression coefficients give the change in the value of a continuous outcome corresponding to a one-unit increase in a covariate. Thus, we can interpret these coefficients as effect sizes of the covariates.

In particular, we estimate (1) logistic regression coefficients for Brazilian Amazon deforestation in 2000–2015, and (2) linear regression coefficients for US tree cover in 2021. We compare the classical method, naive imputation, PPI, stratification, and stratified PPI. Our methods only account for uncertainty in the remotely sensed target variable, while ignoring uncertainty in the covariates; we leave addressing the latter to future work.

### 4.1 Deforestation logistic regression

**Problem Formulation** We estimate the logistic regression coefficients for the association between Brazilian Amazon deforestation in 2000–2015 and several covariates: distance from major roads, distance from major rivers, elevation, and slope (Figure 10). We use logistic regression because the outcome variable (deforested or non-deforested) is binary.

Given  $n$  data points, the logistic regression model is

$$\log \frac{p}{1-p} = \theta_{\text{road}} x_{\text{road}} + \theta_{\text{river}} x_{\text{river}} + \theta_{\text{elevation}} x_{\text{elevation}} + \theta_{\text{slope}} x_{\text{slope}}$$

where  $p$  is a  $n \times 1$  vector of probabilities,  $x_j$  is a  $n \times 1$  vector of covariate  $j$ , and  $\theta_j$  is the scalar logistic regression coefficient for covariate  $j$ . We wish to estimate the  $\theta_j$ . A one-unit increase in covariate  $j$  corresponds to a  $\theta_j$  change in the log-odds of the outcome variable.

We use the same Brazilian Amazon deforestation datasets as the previous section, with  $n = 1386$  ground truth points and  $N = 963548$  uniformly randomly sampled map product points. For the covariates, we use a map of Brazilian federal roads in 2000 [8] and the WWF HydroSHEDS Free Flowing Rivers Network map [14] (we include all rivers of order at most 3) to compute the distance from each data point to the nearest major road and major river. We obtain elevation and slope from the NASA Digital Elevation Model [20] at 30 m resolution. Prior work has shown that deforestation in the Brazilian Amazon is more likely to occur near major roads and navigable rivers due to human settlement and economic activities along these transportation networks [22, 21, 30]. Elevation and slope have also been associated with forest cover change; for example, deforestation is generally less likely on sloped terrain [31]. We do not include a comprehensive list of covariates that could influence deforestation, because the primary purpose of this regression is to illustrate uncertainty quantification rather than explain deforestation.

**Results** The 95% confidence intervals for the four logistic regression coefficients are shown in Figure 11.

The general degree of uncertainty in estimating the coefficients from our non-imputation methods are as follows. The log odds of deforestation change by about  $-.016$  to  $-.010$  for each one-kilometer increase in distance from roads,  $-.008$  to  $-.001$  for each one-kilometer increase in distance from rivers,  $-3$  to  $0.8$  for each one-kilometer increase in elevation, and  $-0.28$  to  $-0.11$  for each one-degree increase in slope. Thus, deforestation is *negatively* associated with all covariates except for elevation. The elevation coefficient confidence intervals intersect with zero for all non-imputation methods except for stratified PPI, suggesting that there might be no association between elevation and deforestation after accounting for the other three variables.

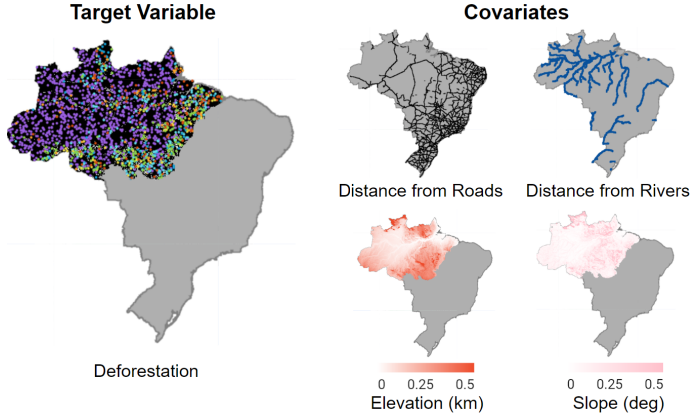


Figure 10: **Brazilian Amazon deforestation logistic regression datasets.** We regress the deforestation binary target variable (left) against four continuous covariates (right): distance from roads, distance from rivers, elevation, and slope.

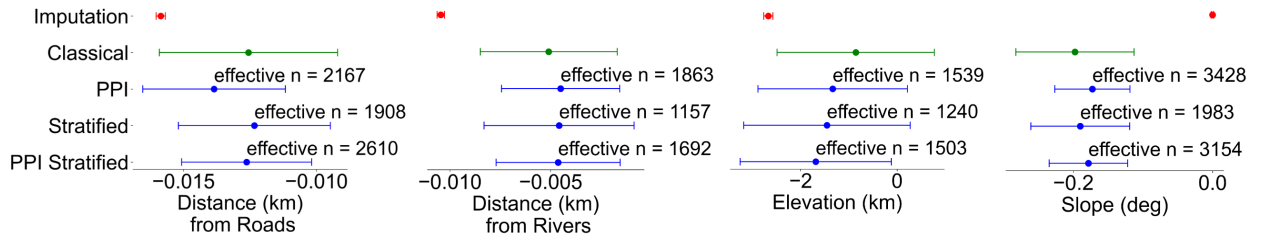


Figure 11: **Brazilian Amazon deforestation logistic regression coefficient 95% confidence intervals** using  $N = 963548$  map product points and  $n = 1386$  ground truth points. The PPI methods result in the smallest confidence intervals, while stratification is not generally effective. For slope and distance from rivers, the map-imputed coefficient falls outside the confidence intervals for all methods that use ground truth points.

The PPI methods result in the smallest confidence intervals, with effective sample size outperforming the classical method by a factor of 1.1 to 2.5 depending on the covariate. The most significant improvement is for the slope covariate. Unlike in our previous area estimation examples, stratification (i.e., weighted logistic regression with weights determined by the strata) is not effective and even reduces effective sample size relative to the classical method when estimating the coefficients for elevation and distance from rivers. Similarly, stratified PPI has slightly worse performance than PPI for all covariates except distance from roads. The strata were designed to minimize variance in deforestation status, which does not necessarily correspond to better estimates of regression coefficients for the covariates.

For slope and distance from rivers, the imputed coefficient computed from the map product falls outside the confidence intervals for all methods that use ground truth points. The imputed coefficient for slope is about 0, and the imputed coefficient for distance from rivers is about  $-0.010$ . In particular, for the slope coefficient, the methods that use ground truth points find an association that is statistically significantly different from zero. However, if we had used only the remote sensing map, we would not have discovered the negative relationship between slope and deforestation. Thus, using only the map product could result in misleading conclusions due to biases in the deforestation map product that are correlated with covariates (e.g., the map product overestimates deforestation at locations with high slope, or underestimates deforestation at locations with low slope).

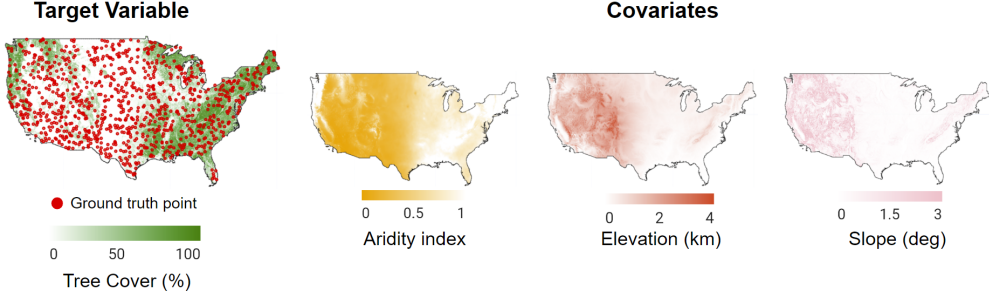


Figure 12: **US tree cover linear regression datasets.** We regress the tree cover percentage target variable (left) against three covariates (right): aridity index, elevation, and slope. We use the USFS Tree Canopy Cover map product and  $n = 983$  uniformly randomly sampled ground truth points.

## 4.2 Tree cover linear regression

**Problem Formulation** Lastly, we estimate linear regression coefficients for the association between 2021 tree cover percentage in the contiguous United States and several covariates: aridity index, elevation, and slope.

Given  $n$  data points, the linear regression model is

$$\mu = \theta_{\text{aridity}} x_{\text{aridity}} + \theta_{\text{elevation}} x_{\text{elevation}} + \theta_{\text{slope}} x_{\text{slope}}$$

where  $\mu$  is a  $n \times 1$  vector of predictions,  $x_j$  is a  $n \times 1$  vector of covariate  $j$ , and  $\theta_j$  is the scalar linear regression coefficient for covariate  $j$ . We wish to estimate the  $\theta_j$ . A one-unit increase in covariate  $j$  corresponds to a  $\theta_j$  change in the outcome variable.

We use  $N = 983238$  map product points sampled uniformly at random from the 2021 USFS Tree Canopy Cover (TCC) product [12] at 30 m resolution. The TCC product is derived from Landsat and Sentinel-2 top-of-atmosphere reflectance data, USDA NASS CDL data, and terrain data. Its tree cover percentage predictions are obtained from random forest models trained on reference data from human-labeled high-resolution imagery. For ground truth, we manually label  $n = 983$  high-resolution satellite images from Google Maps for tree cover percentage, at locations sampled uniformly at random from the study area. Because the source of ground truth is from a uniform random sample, we do not use any stratified methods.

For the covariates, we use a map of the average Global Aridity Index from 1970-2000 (at 30 arc-seconds resolution) [34] and the NASA Digital Elevation Model [20] (at 30 m resolution). The aridity index is defined as a ratio between precipitation and evapo-transpiration, and is *lower* for more arid areas; its value ranges from 0.02 to 6.55 in our dataset. Increased aridity is associated with lower tree cover (and decreased vegetation in general) [5, 39, 6]. Elevation and slope have also been associated with tree cover globally; there is generally more tree cover at lower elevations (e.g., due to higher temperatures) [23] and on sloped terrain [31]. We do not include a comprehensive list of covariates that could influence tree cover, because the primary purpose of this regression is to illustrate uncertainty quantification rather than explain tree cover.

**Results** The 95% confidence intervals for the four linear regression coefficients are shown in Figure 13.

The PPI confidence intervals for coefficients are as follows. Tree cover percentage increases by 35 to 40 percentage points for each one-unit increase in aridity index, decreases by 2.4 to 4.8 percentage points for each one-kilometer increase in elevation, and increases by 0.9 to 1.3 percentage points for each one-degree increase in slope. The PPI effective sample size outperforms the classical method by a factor of 3.3 for aridity index, 2.4 for elevation, and 3.6 for slope. As in the other use cases, PPI uses the map product along with the ground truth to reduce uncertainty in the coefficient estimates compared to only using ground truth.

For elevation, the imputed coefficient computed from the map product ( $-5.3$ ) falls outside the PPI confidence interval. This implies that there is bias in the tree cover map product’s association with elevation (e.g., the map product overestimates tree cover at low elevation locations or underestimates tree cover at high elevation locations). Similar to the deforestation logistic regression use case, using only the map product could result in misleading conclusions. If we had used only the remotely sensed tree cover predictions, we

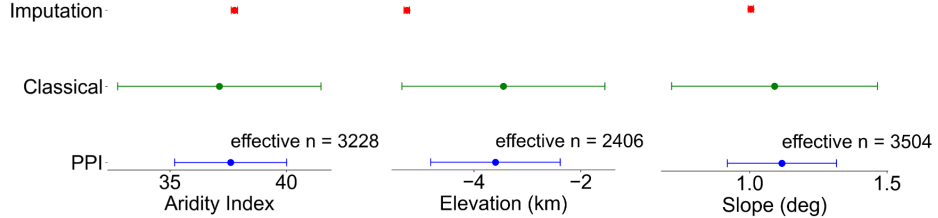


Figure 13: **US tree cover linear regression coefficient 95% confidence intervals** using  $N = 983238$  map product points and  $n = 983$  ground truth points. PPI outperforms the classical method. For elevation, the map-imputed coefficient falls outside the PPI confidence interval.

would have overestimated the magnitude of the relationship between elevation and tree cover due to map errors.

## 5 Discussion

Using remote sensing-based maps to draw scientific inferences requires uncertainty quantification and propagation of uncertainty to downstream analyses — otherwise, we risk making, in the words of [24], just pretty pictures. In this work, we applied several methods that use remote sensing map products, along with a small amount of ground truth data, to estimate area and regression coefficients while correctly taking into account the errors in the map products. We find that stratified sampling, prediction-powered inference, and (for area estimation) the Olofsson method result in lower uncertainty than classical estimates using only ground truth data sampled. Unlike naive imputation using the map product alone, these estimates are guaranteed to be statistically valid.

**Bias is the main issue for naive imputation.** Our experiments illustrated that a naive imputation of area or regression coefficients from a map without bias correction can yield incorrect inferences, and we differentiated between the influence of noise versus bias. In our simulation estimating maize fraction, naive imputation deviated from the true maize fraction of 0.35 as the bias of the crop type map increased. Furthermore, accuracy is not necessarily a good proxy for bias; even at seemingly high map accuracies (accuracy  $> 0.85$ ), naive imputation estimated maize fraction at 0.21 (a 40% underestimate).

In our experiments on real data, imputation for deforestation in the Brazilian Amazon fell within stratified and PPI confidence intervals, suggesting an overall low-bias map product. However, imputation of the logistic regression coefficients on distance from rivers and slope fell outside the intervals computed through the classical, stratified, PPI, and stratified PPI methods. Naive imputation would have concluded that distance from rivers is significantly more predictive of deforestation than it actually is, and that slope has no relationship to deforestation when it actually does. Thus, even when a map product is unbiased for the average outcome, it can be biased for the purpose of estimating regression coefficients. Similarly, imputation of the elevation coefficient in our linear regression for tree cover also overestimates the effect of elevation compared to PPI.

**Effect of map accuracy.** How much stratified sampling, PPI, and confusion matrix-based methods reduce uncertainty relative to classical estimates depends on the quality of the map product. In stratification, the strata map should be designed such that the variance of the quantity of interest is low within each stratum. In PPI (and the Olofsson method), the variance of the difference between the map product predictions  $\hat{Y}$  and the ground truth values  $Y$  should be low. In our maize fraction experiments, a highly accurate map (accuracy = 0.96) was equivalent to having nearly  $6 \times$  as much ground truth data, whereas a low-accuracy map (accuracy = 0.73) only increased the effective sample size by 1.2.

**Stratification vs. PPI vs. Olofsson.** Comparing stratified sampling, PPI, and the Olofsson method, which estimator yields the smallest confidence intervals depends on how the strata were designed and the

quality of the map product. Recall Table 2, which summarizes the conditions under which each method is most appropriate. Empirically, when estimating deforestation fraction in the Brazilian Amazon, we observed the smallest confidence intervals when stratification was used alone or in conjunction with PPI. This is a result of well-designed strata based on a remote sensing map of forest disturbance categories. PPI and the Olofsson method yielded comparable interval widths to each other. This is expected, as the Olofsson method yields similar confidence intervals as PPI when  $N$  is large (Appendix A).

The picture changes, however, when we reuse the same stratified samples to estimate regression coefficients in regressions that the strata were not designed for. When we associated deforestation with covariates in a logistic regression, PPI and stratified PPI resulted in narrower confidence intervals than the stratified estimator across all 4 coefficients (distance from road, distance from river, elevation, and slope). The worse performance of the stratified estimator is because the strata were designed to minimize the variance of deforestation within each strata, which does not necessarily correspond to better regression estimation. Indeed, the stratified estimator was actually worse than the classical estimator for certain coefficients.

An advantage of PPI compared to stratification, then, is its flexibility. While stratification requires us to choose a map product before sampling, PPI can be applied to any map product and any randomly sampled ground truth dataset. Given the expensive nature of ground truth data collection, sampling without choosing a strata map and then using PPI to obtain valid confidence intervals may result in the best performance across a variety of downstream use cases. Or, if stratified samples are already available from area estimation, they can be combined with PPI to estimate regression coefficients.

**Recommendations for map producers and users.** Ultimately, the best methods combine map products with ground truth to yield the narrowest intervals (highest certainty). We recommend that producers of machine learning-generated remote sensing maps use a holdout ground truth dataset for uncertainty quantification. The criterion for this holdout set is that the model, including during hyperparameter tuning, was not trained on it; a standard test set would be adequate. Map producers should release this ground truth data alongside their map product to make their map suitable for downstream scientific inferences. In the absence of a provided holdout set (currently, releasing ground truth data is not the norm), we recommend that map users generate their own ground truth data for the variable of interest if possible.

**Limitations.** All of the estimation methods described in this paper (except for naive imputation) are limited to areas in which ground truth data is available. However, this would be true for any assumption-free, data-driven method that quantifies uncertainty and corrects for map bias. Furthermore, we can only ensure statistical validity of our estimates when the ground truth points are randomly sampled. Together, these attributes mean that such methods may be especially straightforward to use when ground truth data can be generated *de novo*, such as from human inspection of available satellite imagery, and more challenging to use when ground truth data requires bespoke surveys. Another limitation is that our estimates only quantify uncertainty in the target variable map product, and do not account for noise in either the ground truth data or (in the regression use cases) the covariates. We leave these investigations to future work.

## 6 Acknowledgments

This material is based upon work supported by the U.S. Department of Energy, Office of Science, Office of Advanced Scientific Computing Research, Department of Energy Computational Science Graduate Fellowship under Award Number(s) DE-SC0023112. This report was prepared as an account of work sponsored by an agency of the United States Government. Neither the United States Government nor any agency thereof, nor any of their employees, makes any warranty, express or implied, or assumes any legal liability or responsibility for the accuracy, completeness, or usefulness of any information, apparatus, product, or process disclosed, or represents that its use would not infringe privately owned rights. Reference herein to any specific commercial product, process, or service by trade name, trademark, manufacturer, or otherwise does not necessarily constitute or imply its endorsement, recommendation, or favoring by the United States Government or any agency thereof. The views and opinions of authors expressed herein do not necessarily state or reflect those of the United States Government or any agency thereof.

## References

- [1] Jennifer Alix-Garcia and Daniel L Millimet. “Remotely incorrect? Accounting for nonclassical measurement error in satellite data on deforestation”. In: *Journal of the Association of Environmental and Resource Economists* 10.5 (2023), pp. 1335–1367.
- [2] Anastasios N Angelopoulos, John C Duchi, and Tijana Zrnic. “PPI++: Efficient prediction-powered inference”. In: *arXiv preprint arXiv:2311.01453* (2023).
- [3] Anastasios N Angelopoulos et al. “Prediction-powered inference”. In: *Science* 382.6671 (2023), pp. 669–674.
- [4] A. Baccini et al. “Estimated carbon dioxide emissions from tropical deforestation improved by carbon-density maps”. In: *Nature Climate Change* 2.3 (2012), pp. 182–185.
- [5] Jean-François Bastin et al. “The extent of forest in dryland biomes”. In: *Science* 356.6338 (2017), pp. 635–638.
- [6] Miguel Berdugo et al. “Global ecosystem thresholds driven by aridity”. In: *Science* 367.6479 (2020), pp. 787–790.
- [7] Eric L Bullock et al. “Satellite-based estimates reveal widespread forest degradation in the Amazon”. In: *Global Change Biology* 26.5 (2020), pp. 2956–2969.
- [8] Daniel de Castro Victoria et al. “Transport cost to port though Brazilian federal roads network: Dataset for years 2000, 2005, 2010 and 2017”. In: *Data in brief* 36 (2021), p. 107070.
- [9] Jillian M Deines, Sherrie Wang, and David B Lobell. “Satellites reveal a small positive yield effect from conservation tillage across the US Corn Belt”. In: *Environmental Research Letters* 14.12 (Dec. 2019), p. 124038.
- [10] Adam Fisch et al. “Stratified Prediction-Powered Inference for Hybrid Language Model Evaluation”. In: *arXiv preprint arXiv:2406.04291* (2024).
- [11] Katherine Fitzpatrick-Lins. “Comparison of sampling procedures and data analysis for a land-use and land-cover map”. In: *Photogrammetric Engineering and Remote Sensing* 47.3 (1981), pp. 343–351.
- [12] USDA Forest Service. “USFS Tree Canopy Cover v2021.4 (Conterminous United States and South-eastern Alaska)”. In: *Salt Lake City, Utah* (2023).
- [13] Matthew Gordon et al. “Remote control: Debiasing remote sensing predictions for causal inference”. In: *Proc. Int. Conf. Learn. Represent. Workshops.* 22. 2023.
- [14] Günther Grill et al. “Mapping the world’s free-flowing rivers”. In: *Nature* 569.7755 (2019), pp. 215–221.
- [15] World Bank Group. *Mainstreaming the use of remote sensing data and applications in operational contexts*. World Bank, 2018.
- [16] M. C. Hansen et al. “High-Resolution Global Maps of 21st-Century Forest Cover Change”. In: *Science* 342.6160 (2013), pp. 850–853.
- [17] Alan M Hay. “Sampling designs to test land-use map accuracy”. In: *Photogrammetric Engineering and Remote Sensing* 45.4 (1979), pp. 529–533.
- [18] United Nations Satellite Imagery and Geospatial Data Task Team. *Earth Observations for Official Statistics*. United Nations, 2017.
- [19] Meha Jain. “The benefits and pitfalls of using satellite data for causal inference”. In: *Review of Environmental Economics and Policy* (2020).
- [20] NASA JPL. “NASADEM Merged DEM Global 1 arc second V001 [Data set]”. In: *NASA EOSDIS Land Processes DAAC* (2020).
- [21] Kathryn R Kirby et al. “The future of deforestation in the Brazilian Amazon”. In: *Futures* 38.4 (2006), pp. 432–453.
- [22] William F Laurance et al. “Predictors of deforestation in the Brazilian Amazon”. In: *Journal of biogeography* 29.5-6 (2002), pp. 737–748.

- [23] Jordan R Mayor et al. “Elevation alters ecosystem properties across temperate treelines globally”. In: *Nature* 542.7639 (2017), pp. 91–95.
- [24] Ronald E. McRoberts. “Satellite image-based maps: Scientific inference or pretty pictures?” In: *Remote Sensing of Environment* 115.2 (2011), pp. 715–724. ISSN: 0034-4257.
- [25] USDA NASS. “USDA national agricultural statistics service cropland data layer”. In: *USDA-NASS, Washington, DC* (2024).
- [26] Pontus Olofsson et al. “Good practices for estimating area and assessing accuracy of land change”. In: *Remote sensing of Environment* 148 (2014), pp. 42–57.
- [27] Pontus Olofsson et al. “Making better use of accuracy data in land change studies: Estimating accuracy and area and quantifying uncertainty using stratified estimation”. In: *Remote Sensing of Environment* 129 (2013), pp. 122–131.
- [28] Peter Potapov et al. “Global maps of cropland extent and change show accelerated cropland expansion in the twenty-first century”. In: *Nature Food* 3.1 (2022), pp. 19–28.
- [29] Jonathan Proctor, Tamara Carleton, and Sandy Sum. *Parameter recovery using remotely sensed variables*. Tech. rep. National Bureau of Economic Research, 2023.
- [30] Isabel MD Rosa et al. “Predictive modelling of contagious deforestation in the Brazilian Amazon”. In: *PLoS one* 8.10 (2013), e77231.
- [31] Brody Sandel and Jens-Christian Svenning. “Human impacts drive a global topographic signature in tree cover”. In: *Nature Communications* 4.1 (2013), p. 2474.
- [32] Stephen V Stehman and Raymond L Czaplewski. “Design and analysis for thematic map accuracy assessment: fundamental principles”. In: *Remote sensing of environment* 64.3 (1998), pp. 331–344.
- [33] J Townshend. “Global Forest cover change (GFCC) tree cover multi-year global 30 m V003”. In: *NASA EOSDIS Land Processes DAAC* (2016), pp. 176–184.
- [34] Antonio Trabucco. “Global aridity index and potential evapotranspiration (ET0) climate database v2”. In: *CGIAR Consort Spat Inf* (2019).
- [35] Denis Valle, Rafael Izquierdo, and Rodrigo Vieira Leite. “Quantifying uncertainty in land-use land-cover classification using conformal statistics”. In: *Remote Sensing of Environment* 295 (2023), p. 113682.
- [36] Zander S Venter et al. “Uncertainty audit for ecosystem accounting: Satellite-based ecosystem extent is biased without design-based area estimation and accuracy assessment”. In: *Ecosystem Services* 66 (2024), p. 101599.
- [37] Zander S Venter et al. “Global 10 m land use land cover datasets: A comparison of dynamic world, world cover and esri land cover”. In: *Remote Sensing* 14.16 (2022), p. 4101.
- [38] Mengqiu Wang et al. “The great Atlantic Sargassum belt”. In: *Science* 365.6448 (2019), pp. 83–87.
- [39] A Park Williams et al. “Forest responses to increasing aridity and warmth in the southwestern United States”. In: *Proceedings of the National Academy of Sciences* 107.50 (2010), pp. 21289–21294.

## Appendix A Mathematical comparison of PPI and the method of Olofsson

We show that when the number of map product points  $N$  is large, the PPI and Olofsson area estimation confidence intervals are similar. In particular, we show (1) that they have approximately the same length when the number of samples is large and (2) they are centered on the same point. These two facts together provide a mathematical explanation for why PPI and the Olofsson method approximately agree in all of our experiments.

We begin with notation. Estimating the area proportion of a land cover class in a given region is equivalent to estimating the mean of a binary variable  $Y$ , where  $Y = 1$  for points in the class and  $Y = 0$  for points outside the class. Suppose we have  $n$  uniformly random sampled ground truth points  $Y_1, Y_2, \dots, Y_n$  and  $N$  map product points  $\hat{Y}_1, \hat{Y}_2, \dots, \hat{Y}_N$ . For all  $0 \leq i, j \leq 1$ , let  $n_{ij}$  denote the number of ground truth points that are in both map class  $i$  and ground truth class  $j$ . Let  $n_{\cdot i} = n_{i0} + n_{i1}$  denote the total number of ground truth points in map class  $i$ , and  $n_{i\cdot} = n_{0i} + n_{1i}$  denote the total number of ground truth points in ground truth class  $i$ . Furthermore, let  $A_i$  denote the fraction of the map product that is in class  $i$ . We have  $A_0 + A_1 = 1$ . The map-imputed area estimate, which we will correct for bias, is  $A_1$ . We will use the approximations  $A_0 \approx \frac{n_{0\cdot}}{n}$  and  $A_1 \approx \frac{n_{1\cdot}}{n}$ . This is a reasonable approximation since the  $n$  ground truth locations are sampled uniformly at random.

With this notation, we have the following,

$$\begin{aligned} \sum_{i=1}^n Y_i &= n_{\cdot 1} \\ \sum_{i=1}^n \hat{Y}_i &= n_{1\cdot} \\ \text{Var}_n(Y) &= \frac{n_{\cdot 0} n_{\cdot 1}}{n^2} \\ \text{Var}_N(\hat{Y}) &= A_0 A_1 \approx \frac{n_{0\cdot} n_{1\cdot}}{n^2} \text{ and} \\ \text{Cov}_n(Y, \hat{Y}) &= \frac{n_{00} n_{11} - n_{01} n_{10}}{n^2}. \end{aligned}$$

**Standard errors.** We now turn to the PPI standard error. We have

$$\begin{aligned} SE_{\text{PPI}} &\rightarrow \sqrt{\frac{1}{n} \text{Var}(Y - \lambda \hat{Y})} && \text{since } N \gg n \\ &= \sqrt{\frac{1}{n} \left( \text{Var}(Y) + \lambda^2 \text{Var}(\hat{Y}) - 2\lambda \text{Cov}(Y, \hat{Y}) \right)} && \text{expanding out } \text{Var}(Y - \lambda \hat{Y}) \\ &\rightarrow \sqrt{\frac{1}{n} \left( \text{Var}(Y) - \frac{\text{Cov}(Y, \hat{Y})^2}{\text{Var}(\hat{Y})} \right)} && \text{plugging in } \lambda \\ &\approx \sqrt{\frac{1}{n} \left( \frac{n_{\cdot 0} n_{\cdot 1}}{n^2} - \frac{(n_{00} n_{11} - n_{01} n_{10})^2}{n^2 n_{0\cdot} n_{1\cdot}} \right)} && \text{plugging in } \text{Var}(Y), \text{Var}(\hat{Y}), \text{Cov}(Y, \hat{Y}) \\ &= \sqrt{\frac{1}{n^2 n_{0\cdot} n_{1\cdot}} (n_{01} n_{00} n_{10} + n_{01} n_{00} n_{11} + n_{11} n_{10} n_{00} + n_{11} n_{10} n_{01})} && \text{using algebraic manipulation.} \end{aligned}$$

Above, we use the fact that as  $n, N \rightarrow \infty$ , the PPI tuning parameter (from Example 6.1 of [2]) behaves as

$$\lambda \rightarrow \frac{\text{Cov}_n(Y, \hat{Y})}{\text{Var}_N(\hat{Y})} \approx \frac{n_{00} n_{11} - n_{01} n_{10}}{n_{0\cdot} n_{1\cdot}}.$$

We compare this with the Olofsson standard error

$$\begin{aligned}
SE_{\text{Olofsson}} &= \sqrt{A_0^2 \frac{\frac{n_{00}}{n_{0.}} \frac{n_{01}}{n_{0.}}}{n_{0.}} + A_1^2 \frac{\frac{n_{10}}{n_{1.}} \frac{n_{11}}{n_{1.}}}{n_{1.}}} \\
&\approx \sqrt{\left(\frac{n_{0.}}{n}\right)^2 \times \frac{\frac{n_{00}}{n_{0.}} \frac{n_{01}}{n_{0.}}}{n_{0.}} + \left(\frac{n_{1.}}{n}\right)^2 \times \frac{\frac{n_{10}}{n_{1.}} \frac{n_{11}}{n_{1.}}}{n_{1.}}} \quad \text{plugging in } A_0 \text{ and } A_1 \\
&= \sqrt{\frac{1}{n^2 n_{0.} n_{1.}} (n_{01} n_{00} n_{10} + n_{01} n_{00} n_{11} + n_{11} n_{10} n_{00} + n_{11} n_{10} n_{01})} \quad \text{using algebraic manipulation.}
\end{aligned}$$

The expressions we arrive at for PPI and the method of Olofsson agree, indicating that for large sample sizes the standard errors are approximately equal. This implies that the confidence intervals from the two methods will have the same width.

**Point estimates.** Next, we show that the PPI and Olofsson confidence intervals are centered around the same point. Turning first to the PPI point estimate

$$\begin{aligned}
\hat{\theta}_{\text{PPI}} &= \lambda A_1 - \frac{1}{n} \sum_{i=1}^n (\lambda \hat{Y}_i - Y_i) \\
&\approx \frac{\lambda n_{1.}}{n} - \frac{\lambda n_{1.} - n_{.1}}{n} \quad \text{plugging in } A_1, \sum_{i=1}^n Y_i, \text{ and } \sum_{i=1}^n \hat{Y}_i \\
&= \frac{n_{.1}}{n}
\end{aligned}$$

The Olofsson area point estimate is

$$\begin{aligned}
\hat{\theta}_{\text{Olofsson}} &= A_0 \frac{n_{01}}{n_{0.}} + A_1 \frac{n_{11}}{n_{1.}} \\
&\approx \frac{n_{0.}}{n} \times \frac{n_{01}}{n_{0.}} + \frac{n_{1.}}{n} \times \frac{n_{11}}{n_{1.}} \quad \text{plugging in } A_0 \text{ and } A_1 \\
&= \frac{n_{.1}}{n}
\end{aligned}$$

We see that the final expressions are equal, which means the point estimates are approximately equal.

## Appendix B Binarizing the NASA Global Forest Cover Change map product for deforestation

In the Brazilian Amazon deforestation use cases, the ground truth points from [7] have binary deforestation values ( $Y = 1$  if deforested and  $Y = 0$  if not deforested between 2000-2015), while the NASA GFCC map product gives canopy cover percentages over time at each pixel.

In order to binarize the continuous map product data, we classify a map pixel as “deforested” if its canopy cover percentage satisfies  $\text{canopy}_{2015} - \text{canopy}_{2000} \leq -25\%$ . We choose the  $-25\%$  threshold by visually comparing the map-derived canopy cover change distributions for deforested and non-deforested ground truth points (Figure 14). Most of the deforested ground truth points have a map canopy cover decrease of more than  $25\%$ , while most of the non-deforested ground truth points have either a map canopy cover increase, no map canopy cover change, or a map canopy cover decrease of less than  $25\%$ .

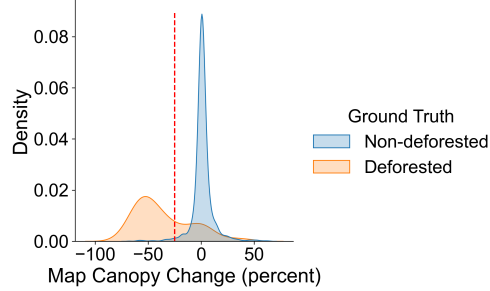


Figure 14: **NASA GFCC map canopy cover change (2000-2015) distributions for non-deforested and deforested ground truth** over  $n = 1386$  uniformly random sampled points. The distributions are visualized using kernel density estimation. We choose a  $-25\%$  deforestation threshold (shown in red) to binarize the map product.